

Soft Matter

Accepted Manuscript



This is an *Accepted Manuscript*, which has been through the Royal Society of Chemistry peer review process and has been accepted for publication.

Accepted Manuscripts are published online shortly after acceptance, before technical editing, formatting and proof reading. Using this free service, authors can make their results available to the community, in citable form, before we publish the edited article. We will replace this *Accepted Manuscript* with the edited and formatted *Advance Article* as soon as it is available.

You can find more information about *Accepted Manuscripts* in the [Information for Authors](#).

Please note that technical editing may introduce minor changes to the text and/or graphics, which may alter content. The journal's standard [Terms & Conditions](#) and the [Ethical guidelines](#) still apply. In no event shall the Royal Society of Chemistry be held responsible for any errors or omissions in this *Accepted Manuscript* or any consequences arising from the use of any information it contains.

Electro-Capillary effects in Capillary Filling Dynamics of Electrorheological Fluids

Jayabrata Dhar, Uddipta Ghosh and Suman Chakraborty

Indian Institute of Technology, Kharagpur, Kharagpur

Soft Matter Accepted Manuscript

suman_mech@iitkgp.ernet.ac.in

Abstract

Flow of electrorheological fluids is characterized by an apparent increase in viscosity manifested by the yield stress property of the fluid, which is a function of applied electric field and concentration of the suspended solute phase within the dielectric medium. This property of electrorheological fluids generally hinders flow through a capillary, if the imposed shear stress is lower than the induced yield stress. This results in a plug-like zone in the flow profile, thus, granting the fluid a Bingham-plastic behavior. In the present work, we study such influences of the yield stress on the capillary filling dynamics of an electrorheological fluid, by employing rheologically consistent reduced order formalism. One important feature of the theoretical formalism is addressing an intricate interplay between the surface tension and viscous forces, both of which depend sensitively on the electric field. Our analysis reveals that the progress of the capillary front is hindered at an intermediate temporal regime, as attributable to the increase of the span of the plug-zone across the channel width with time. With preliminary understanding on the cessation of capillary front advancement due to the yield stress property of the electrorheological fluids, we further strive to achieve a basic comparison with an experimental study made earlier. Reasonable agreements with reported data support our theoretical framework. Comprehensive scaling analysis brings further insight to our reported observations over various temporal regimes.

1. Introduction

Electrorheological fluids (ERFs) are amongst those smart fluids whose flow characteristics can be controlled and manipulated on-the-fly with variations in electric field, since the response of the fluid rheology to this electric field variation is highly spontaneous and reversible¹⁻⁵. ERFs instantly increase their apparent viscosity subject to the application of an external electric field. This apparent increase in viscosity is termed as the ER effect or Winslow effect⁶ (after the name of W. Winslow, who first discovered and attempted to describe the effect on the basis of fibrillation due to chain formation). ERFs have been a subject of ardent interest and have been thoroughly investigated and studied by experimental, theoretical and numerical methods^{1,5,7-13}. ER fluids are generally colloidal suspensions which comprise of two phases; a solvent phase which is basically a dielectric medium and a suspended solute phase of particles whose size ranges from micrometer to tens of nanometers^{1,6}. The basis of the ER effect, which is attributed to the columnar chains formed by the particulate phase on application of an electric field, is described in details in the reviews^{1,4,14} and references therein. The ER effect, in essence, holds immense potential towards modulating the dynamics of capillary flows for on-chip applications, in a rather non-intuitive manner, as attributed to a simultaneous influence of the applied electric field on the driving interfacial tension and opposing viscous resistance.

Over the years, numerous studies have been reported on the capillary filling dynamics of various fluids, which include analytical, semi-analytical as well as experimental investigations¹⁵⁻²⁴. Flow actuation and transport phenomena due to capillary action finds its use in various fields of science and engineering, namely groundwater movement, heat pipes, candle wicks, marker pens, lab-on-a-chip micro-devices, micro-total analysis systems, optical switches, to name a few^{19,25-28}. A basic model governing the transients of the capillary filling and meniscus advancement essentially follows from an interplay of inertial, viscous, surface tension, and gravity forces, leading to a reduced order based mathematical formalism^{18,26}. Extensive studies on different regimes (early inertial regimes, viscous Washburn regimes, etc.) of capillary filling that arise due to the interplay of inertial, viscous and gravitational effects²⁹⁻³¹ have also been reported. Recently, the effects of entrance pressure and unsteady flow effects have been studied, extending the applicability of the lumped model approach³². Although such models cannot

capture the meniscus shape explicitly, their predictions have been shown to agree well with experiments^{25,33,34}.

Despite the fact that majority of the literature on capillary action is focused on Newtonian fluids, capillary filling dynamics of Non-Newtonian fluids has also been studied by a number of researchers^{21,27,34,35}, due to their practical applications in fluids such as polymer solutions and biofluids^{19,26,27,36}. Experiments on capillary filling of ER fluids³⁵ have also been executed in recent years, which demonstrate several non-intuitive trends in the meniscus displacement characteristics. However, a close review of the literature suggests that no suitable theoretical analysis exists, to the best of authors' knowledge, which take ER fluids as the filling medium.

In this work, we focus on theoretical study of capillary filling of an electrorheological fluid through a parallel plate channel. To this end, we apply a reduced order approach to determine the dynamic evolution of the fluid height as function of electric field and particle concentration. We also take into account the effects of electro-capillarity. We consider the classical Bingham model for the ERFs, which finds diverse use for modeling of electrorheological flows^{1,37} and successfully matches with experimental findings. We compare our results with the previously reported experiments on capillary filling of ERFs and show that reasonably good agreement is observed between the two, within the constraints of lumped parameter based approximations. We further offer a comprehensive scaling analysis, in an effort to establish the characteristics of various temporal regimes of the capillary filling dynamics.

2. Mathematical formulation

Figure 1 describes a conceptual schematic of the capillary advancement and figurative details of the present study. We consider the parallel plates to act as electrodes, when an electric field is applied. Since the ER fluid is itself a dielectric medium, it does not require a dielectric layer for insulation from the electrodes. The axial direction of the parallel plates is considered to run along the x direction, while the perpendicular direction is considered to run along the y direction. It must, however, be noted that ER fluids, as considered in the present study, generally comprise dielectric particles suspended in an organic medium. Since the medium has an extensively low conductivity, the presence of any electrical double layer (EDL)^{38,39} and their effects on the capillary dynamics may be safely ruled out. Nevertheless, studies have been reported in the

literature where influence of the association of EDL with the capillary transport has been looked into⁴⁰, albeit for Newtonian fluids.

As mentioned earlier, description of the capillary filling dynamics heavily relies on a description of the viscous resistance, which in turn depends on the flow field under consideration. Before attempting to solve for the flow dynamics, we shall first find an appropriate relationship of the resulting yield stress as a function of the applied electric field and particle concentration.

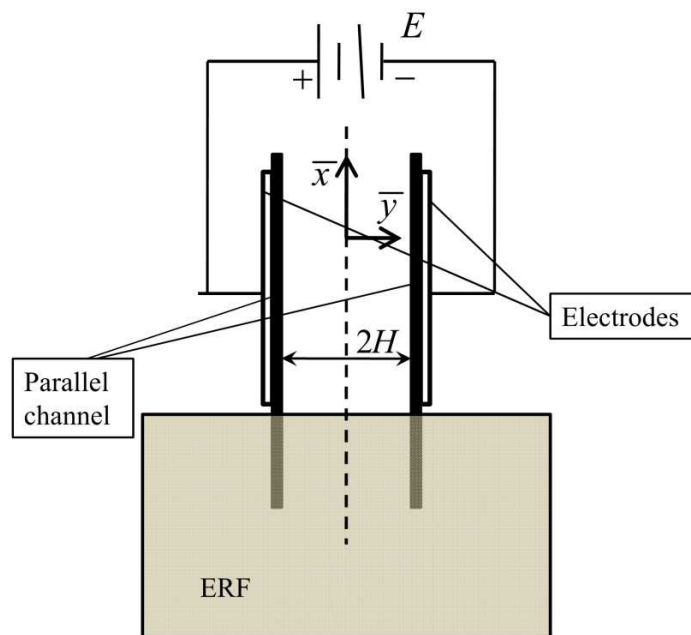


Fig 1. The schematics of the capillary rise of the ERF through the parallel channel

2.1. The yield stress

The phenomena of Bingham-like nature of ER fluids with a characteristic yield stress are specifically attributed to the formation of columnar chain-like structures of the solute particles across the electrode in presence of an external electric field^{1,2,14}. The strength of the yield stress depends on the field strength and solute concentration. Various studies have been put forward to quantify this parameter in the scope of mean-field approximation^{1,41-43}. While the Dielectric Electrorheological (DER) fluids show a quadratic dependence of yield stress on the electric field, Giant Electrorheological (GER) fluids have a linear variation of the same^{1,3,4,44}. Alongside the field-dependant yield stress, it has also been seen that the solute concentration has a drastic

influence on the yield-like nature of the ER fluids^{1,41}. The yield stress generally increases with particle concentration and attains a maximum at large concentrations¹. These observations have led to many theories quantifying the yield stress with experimental verification. One such popular generalized theory accounts for both the field and particle concentration dependency and is given by the form^(1,41):

$$\tau_0 = 18\phi \operatorname{Re}(\varepsilon_c) \varepsilon_0 \beta^2 E^2 f_m \left(1 - \frac{(\pi/6)^{1/2}}{(l/a) \tan \theta_m \phi^{1/2}} \right) \quad (1)$$

where τ_0 denotes yield stress of the ER fluid, ϕ is the solute volume fraction, ε_p and ε_c denote the complex effective permittivity of the particular and continuous phase, respectively; $\operatorname{Re}(\varepsilon_c)$ is the real part of the effective permittivity (dielectric constant) of the medium, E is the electric field, $2H$ is the channel height, ε_0 is the absolute permittivity of the vacuum and a is the particle radius. β is the Clausius-Mossotti factor which is given by $\beta = (\varepsilon_p - \varepsilon_c) / (\varepsilon_p + 2\varepsilon_c)$, while f_m and θ_m are the maximum dimensionless restoring force during the rupture of columnar chains, and the angle at this maximum, respectively. The value range of the CM factor is $-0.5 < \beta < 1$. The values of f_m and θ_m have been evaluated in reference⁴¹. The above formulation, derived considering a DER fluid, holds good for low to moderate volume fractions (between 0.1 and 0.3) of particles.

It is a well established fact that the polarization force between two particles in an electric field is governed by the mismatch of the effective permittivity of the particles and the suspending medium^{4,45,46}. This is one of the most significant mechanisms that governs the electrorheological effect in any particulate suspension. The effective permittivity, in general, consists of three quantities, a real permittivity ε' , an imaginary frequency-dependent dielectric constant (responsible for the dielectric loss) ε'' and an imaginary conductivity part which is also frequency dependent $\sigma' / \varepsilon_0 \omega$, where ω is the angular frequency of the applied electric field and σ' is the conductivity⁴⁵. Therefore, the effective permittivity eventually has the form $\varepsilon = \varepsilon' - j\varepsilon'' + j\sigma' / \varepsilon_0 \omega$, where j is $j = \sqrt{-1}$. The effective permittivity is generally applied to

construct the Classius-Mossotti (CM) factor given by $\beta = \frac{\varepsilon_p - \varepsilon_f}{\varepsilon_p + 2\varepsilon_f}$, where ε_p is the effective

permittivity of the particulate medium and ε_f is the effective permittivity of the fluid medium.

In general, the CM factor is a complex number and describes the real and imaginary contribution of the overall permittivity tensor on the induced dipole moment. This effective dipole moment due to the induced polarization among the particles is given by the expression ⁴⁵

$p = 4\pi \text{Re}(\varepsilon_c) \beta a^3 E_0$, where " a " is the particle radius and ε is the absolute real part of the effective permittivity of the fluid medium. It has been shown in previous studies that when the applied electric field is in DC (no frequency is associated with the field) or low frequency AC mode, the conductivity in the imaginary part of the effective dielectric constant governs the CM factor ⁴⁷, and thereby, the induced dipole moment. In such cases, the dipole moment thus takes

the form: $p = 4\pi \text{Re}(\varepsilon_c) a^3 E_0 \left(\frac{\sigma'_p - \sigma'_c}{\sigma'_p + 2\sigma'_c} \right)$. On the other hand, for a high frequency alternating

field (AC), the real part is more dominant in governing the induced dipole moment magnitude. It must be noted that since our study is carried out in the DC field paradigm, we should consider the effects of the medium conductivities to dominate the polarization effects among the particle chains.

In the present study, the columnar chains are further assumed to be one particle thick for the derivation. Although these approximations are quite gross, they were successful in predicting the yield stress when compared with experimental values ^{1,41}.

2.2. The hydrodynamic equations

We shall use the form in (1), for quantifying the yield stress as a function of the applied field and suspended particulate concentration in the ER media. Following these observations, the generalized stress-strain relationship for an ERF accounting for the yield-like nature is given by

$$\left. \begin{aligned} \tau &= -\tau_0 + \mu \frac{du}{dy}; \frac{du}{dy} < 0 \\ \tau &= \tau_0 + \mu \frac{du}{dy}; \frac{du}{dy} > 0 \end{aligned} \right\}, \text{ if } \tau > \tau_0 \quad (2)$$

$$\frac{du}{dy} = 0, \text{ if } \tau \leq \tau_0$$

The yield stress τ_0 in (2), can be expressed in the mathematical form, as given in (1). In the present work, we have chosen a fluid which comprises micro-particles suspended in an organic medium^{1,37,41}. Such fluids tend to give rise to an yield stress which can closely be described by (1)^{1,41}. It has been shown in various studies that these particulate suspensions also approximately follow the classical Bingham plastic like model (which has been widely adopted for such class of fluids), and exhibit a Newtonian nature after the yield-point is overcome⁴¹. In order to delineate the coupled effects of electro-capillarity and rheological variation in the capillary dynamics of ER fluids, we have proceeded with the classical Bingham model, where the shear viscosity is only considered as the function of the particle concentration. This, in effect, simulates the zero-field Newtonian-type suspension viscosity at high shear regions^{48,49}. The primary motivation for employing such a model is to carry out a simple analysis that could bring out the basic non-linearity and trends in the capillary filling of ER fluids, without sacrificing the essential physics in the problem. In the scope of lumped parameter model^{18,21,34}, we first seek to obtain the velocity profile for a fully developed flow within the parallel plate channel. This velocity profile is essentially needed to describe the viscous resistance during capillary motion. The Cauchy's equation of motion for a steady, laminar pressure driven flow within a parallel microchannel has the form

$$\frac{dp}{dx} = \frac{d\tau}{dy} \quad (3)$$

where $\tau = \tau_{xy}$ is the shear stress in the xy -component of the stress tensor. Integrating equation (3) with a boundary condition of vanishing shear stress at the channel centerline, we arrive at the following equation

$$\tau = \frac{dp}{dx} y \quad (4)$$

Now, inserting equation (2) into equation (4) and using the no-slip boundary condition at the walls $u(y = H) = 0$, we solve for the velocity profile, which takes the form

$$u = -\frac{1}{2\mu} \frac{dp}{dx} (H^2 - y^2) - \frac{\tau_0}{\mu} (H - y) \quad (5)$$

However, there will be a region within the domain cross-section where the shear stress will be less than the yield stress and the velocity profile will experience a plug-like zone. This region can be found with the aid of equations (2) and (4), resulting in an equation of the form

$$-\tau_0 + \mu \frac{du}{dy} = \frac{dp}{dx} y. \quad \text{Since } \frac{du}{dy} = 0 \text{ at the boundary of the plug zone, the span of the plug-zone}$$

from the centerline (denoted by y_1) is simply given by: $y_1 = \tau_0 / \left(-\frac{dp}{dx} \right)$, wherein we notice that the span of the plug zone across the domain is $-y_1 \leq y \leq y_1$. Within the plug zone, the velocity remains constant and has the value

$$u_1 = -\frac{1}{2\mu} \frac{dp}{dx} (H^2 - y_1^2) - \frac{\tau_0}{\mu} (H - y_1) \quad (6)$$

From equation (5) and (6) the average velocity over the cross section of the parallel channel can

be found using the expression $\bar{u} = \frac{2 \left(\int_0^{y_1} u_1 dy + \int_{y_1}^H u dy \right)}{2H}$ which reads:

$$\bar{u} = -\frac{dp}{dx} \frac{(H^3 - y_1^3)}{3H\mu} - \tau_0 \frac{(H^2 - y_1^2)}{2H\mu} \quad (7)$$

Two important points can be noted from the above equations. Straightaway, we can see that the average velocity across the channel shows that it is less than that for Poiseuille flow, due to the presence of the plug-zone near the channel centerline, and thus, the maximum velocity for a parabolic profile is not attained. The second but a more subtle nature is that with a decrease in the pressure gradient (or imposed actuation force on the flow), the average velocity does not depict a linear decrease. This is due to the fact that the width of the plug zone y_1 increases with a

decrease in the pressure according to $y_1 = \tau_0 / -\frac{dp}{dx}$ as discussed above. Therefore, a decrease in pressure gradient increases the effect of the second term on the right hand side of equation (7), thereby decreasing the average velocity further. This intricate nature of the flow will be used in the following discussion of the capillary filling dynamics and its influence on the capillary front cessation.

2.3. The surface tension force: Electro-capillary effect

It has been shown in numerous earlier studies⁵⁰⁻⁵³ that the surface tension depends on a number of external parameters, such as the electric field, and presence of external particles in the liquid phase, both of which alter the interfacial energy, finally resulting in a change in the equilibrium Jurin height. This effect, in presence of an applied electric field, is known as electro-capillary effect, which is quantified by the change in the contact angle at the fluid-fluid-wall interface. Various analytical and experimental studies^{50,54-57} have shown that with an applied electric field, interfacial free energy alters, resulting in a change in the apparent contact angle.

The theory of electrowetting and electrocapillarity has been the topic of numerous studies in the past. Electrowetting effect refers to the apparent decrease in the contact angle the liquid makes with the solid surface. On the other hand, the phenomenon where a net electrochemical force is exerted on a liquid mass by applying an external voltage in a suitable arrangement is sometimes referred to as electrocapillarity⁵⁰. Although these two phenomena are usually grouped together and follow a similar mechanism, they have been distinguished in few recent studies^{50,58}. Although the electrowetting term is restricted to the observable change in the contact angle, the prediction of the electromechanical force responsible for the electrocapillary effect, is consistent with the Young-Lippmann electrowetting theory when Laplace equation is augmented with the electrowetting phenomenon to estimate the net height-of-rise of the liquid. In other words, when we consider the change in contact angle due to the application of electric field according to Young-Lippmann equation, the electrocapillary force automatically gets included in the formulation. To this end, we consider the change in the contact angle, which follows from the basic mechanism of the electrowetting scenario, instead of incorporating the two cumulative surface tension and electrochemical forces in the formulation. Accordingly, with an assumption of absence of any dielectric coating layer and electric field independent liquid-vapor surface

tension coefficient, the Young-Lippmann equation describing the electric field driven wetting characteristics reads,

$$\cos \theta = \cos \theta_0 + \frac{\varepsilon H E^2}{w \sigma} \quad (8)$$

where w is the contribution factor of the capacitive energy term, H is the capillary half-width, E is the applied electric field and $\sigma = \sigma_{lv}$ is the surface tension at the liquid-vapor interface. The factor w has been included in equation (8), in an effort to keep the value of the quantity on the right hand side less than 1. We have chosen the value of w based on experimental readings, as discussed in the comparison with experimental results section. The resultant surface tension force actuating the capillary rise through the narrow conduit is given by the form

$$F_{surf} = 2b\sigma \cos \theta \quad (9)$$

Since the electric field alters the driving surface tension force and the resistive viscous force simultaneously, its implication on the capillary filling dynamics is rather non-trivial, as discussed subsequently.

2.4 Reduced order model

In the scope of the reduced order analysis^{18,21}, the net shear force per unit axial distance at the channel upper-wall is derived from equation (4) with $y = H$ and is given by $F_{w,v} = -\frac{dp}{dx} bH$, with b being the channel width. Similar viscous hindrance is experienced at the bottom wall at $y = -H$. The total viscous force, thus, experienced by the shearing of the fluid near the channel is given by $F_{visc} = 2F_{w,v}x = -2bH \frac{dp}{dx} x$. The pressure gradient is then replaced with the average velocity from equation (7) and the resulting viscous force reads:

$$F_{visc} = 3bHx \left(\frac{\tau_0 (H^2 - y_1^2) + 2\bar{u} \mu H}{H^3 - y_1^3} \right) \quad (10)$$

The gravitational force on the capillary is simply given by:

$$F_{grav} = 2\rho gHx \quad (11)$$

We are now in the position to formulate the governing equation for capillary front advancement, which is the balance of inertial, viscous, gravitational and surface tension forces. The lumped equation of motion is thus given by:

$$2H\rho \frac{d}{dt} \left(x \frac{dx}{dt} \right) = 2\sigma \cos(\theta) - 2\rho gHx - \frac{3 \left(\tau_0 (H^2 - y_1^2) + 2 \frac{dx}{dt} \mu H \right) Hx}{H^3 - y_1^3} \quad (12)$$

where the common factor b , the width of the wall, is cancelled from both sides of the equation and the average velocity \bar{u} is replaced by the rate of meniscus rise dx/dt . This is actually the essence of the reduced order model wherein we approximate the velocity of the advancing meniscus by an average velocity \bar{u} , and replace it with the rate of advancement of the meniscus dx/dt in order to obtain the governing equations for advancement of the meniscus^{16,21,29}. The above equation is now non-dimensionalized using the terms $\bar{x} = x/H$ and $\bar{t} = t/t_0$ where $t_0 = \sqrt{\rho H^3/\sigma}$ is obtained from the balance of the inertial and surface tension effects. The final non-dimensional form of the governing equation then has the form

$$\frac{d}{d\bar{t}} \left(\bar{x} \frac{d\bar{x}}{d\bar{t}} \right) = \cos(\theta) - Bo \cdot \bar{x} - \frac{3}{2} \xi \frac{(1 - \bar{y}_1^2)}{(1 - \bar{y}_1^3)} \bar{x} - \frac{3Ca}{(1 - \bar{y}_1^3)} \bar{x} \left(\frac{d\bar{x}}{d\bar{t}} \right) \quad (13)$$

where $\bar{y}_1 = y_1/H$ denotes the non-dimensional span of the plug zone, $Bo = \frac{\rho g H^2}{\sigma}$ is the gravitational Bond number, $\xi = \frac{H\tau_0}{\sigma}$ denotes a dimensionless number representing the ratio between the polarization energy to surface energy and $Ca = \frac{\mu}{\sqrt{\rho\sigma H}} = \frac{\mu H}{\sigma t_0}$ denotes the characteristic capillary number for the flow.

A prior knowledge of the evolution of the plug zone dimension, which is a function of the velocity (and thus, a function of time), is necessary for the progressive solution of the

problem. The span of the plug zone can be estimated from $\bar{y}_1 = \tau_0 / -H \frac{dp}{dx}$, which can now be recast into the cubic form

$$0 = \bar{y}_1^3 - 3\bar{y}_1 - 6\bar{y}_1 Mn \frac{d\bar{x}}{dt} + 2 \quad (14)$$

where $Mn = \frac{Ca}{\xi} = \frac{\mu}{\tau_0 t_0}$ denotes the modified Mason number for the system. This definition of the Mason number ensures that equation (14) is coupled with the dimensionless governing flow equation (13). The Jurin height is estimated from equation (12) by substituting the inertial and viscous terms to zero, and has the form

$$J = \frac{\sigma \cos(\theta)}{\rho g H + \frac{3}{2} \tau_0 \left(\frac{1 - \bar{y}_1^2}{1 - \bar{y}_1^3} \right)} \quad (15)$$

As the value of \bar{y}_1 approaches 1, the factor $\left(\frac{1 - \bar{y}_1^2}{1 - \bar{y}_1^3} \right)$ approaches to a value $\frac{2}{3}$. Therefore, an asymptotic close approximation of the value of the dimensionless equilibrium Jurin height (given by $\bar{J} = J/H$) can take the form

$$\bar{J} = \frac{\cos(\theta)}{Bo + \xi} \quad (16)$$

The Newtonian counterpart of the capillary rise governing equation and the Jurin height is given as

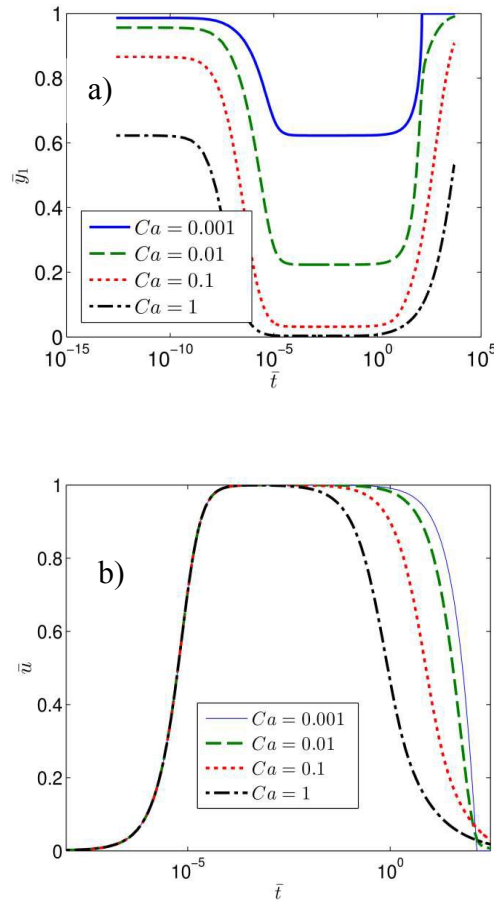
$$\frac{d}{dt} \left(\bar{x} \frac{d\bar{x}}{dt} \right) = \cos(\theta) - \frac{\rho H^2 g}{\sigma} \bar{x} - \frac{3\mu H}{t_0 \sigma} \bar{x} \frac{d\bar{x}}{dt} \quad (17)$$

$$\bar{J}_N = \frac{\cos(\theta)}{Bo}$$

where a similar non-dimensional scheme with $\bar{x} = x/H$, $\bar{t} = t/t_0$ and $t_0 = \sqrt{\rho H^3 / \sigma}$ is used.

3. Results and discussions

Equation (13) has been solved numerically using Runge-Kutta method^{59,60}, subject to the following initial conditions; $\bar{x}(0) \rightarrow 0$ and $\frac{d\bar{x}}{d\bar{t}}(0) = 10^{-6}$. We consider a very small velocity at the time of capillary entry to avoid for the plug zone completely spanning the channel. This can be justified on the basis that the electric field is applied just after the fluid starts to enter the capillary, or else the fluid motion will cease at the entry plane. For representative numerical calculations, the height of the channel is assumed in the order of 1mm while the viscosity of the particulate medium is assumed to be of the order of 10^{-2} Pa-s. The density of the carrier fluid is considered as 1000 kg/m^3 and the yield stress is assumed to have a value in order of 10 Pa. We have considered the value of static contact angle as 30° .



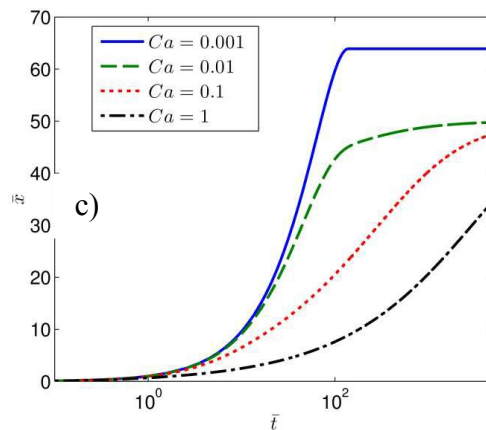
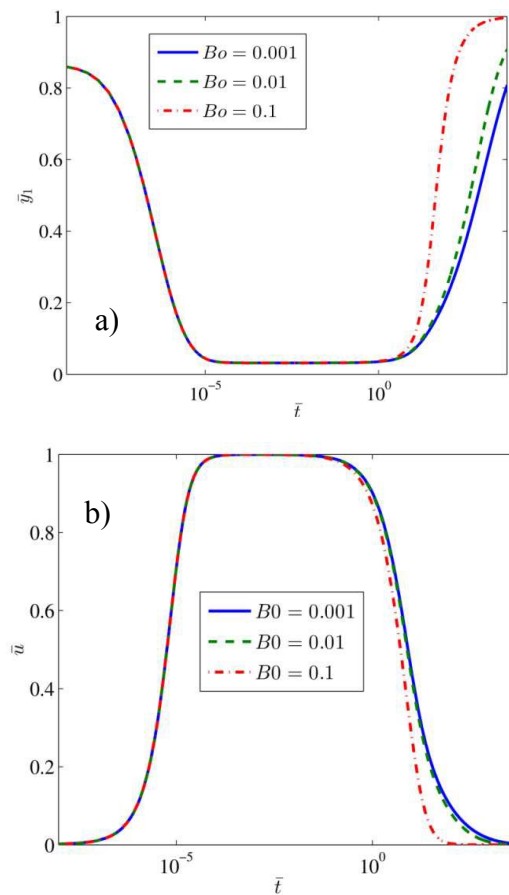


Fig 2. Figure represents the a) development of the dimensionless span of the plug zone \bar{y}_1 measured from the channel centerline; b) variation of dimensionless average velocity of the capillary front \bar{u} ; and c) capillary front advancement \bar{x} as a function of the dimensionless time \bar{t} for different values of characteristic capillary number Ca . The other dimensionless parameters are $Bo = 0.01$; $\xi = 0.01$

Figures 2.(a) – 2.(c) depict the variation of span of the plug zone (fig a), the resulting meniscus velocity (fig b) and the position of the capillary front as functions of time for different values of Ca (fig c), while the other relevant parameters have been mentioned in the caption. Figure 2a shows that the plug zone spans nearly across the whole channel at the beginning of the capillary filling. This is due to the initial low velocity of the capillary front since the inertial effects are dominant in this regime. This lower velocity results in lower shear stresses. Since, this stress is lower than the yield stress value in most parts of the channel except near the channel walls, a plug zone spanning nearly across the whole channel is observed. As the velocity increases with time (see figure 2b), a larger shear rate is induced across the channel decreasing the span of the plug zone. With the meniscus penetrating more into the capillary, the viscous effects naturally become more dominant. This slows down the flow and hence the plug zone span again starts to increase. Once it spans across the whole channel, any further advancement of the capillary front is arrested and the meniscus reaches the equilibrium position. As the capillary number increases, the effect of the viscous drag on the capillary front increases. This lowers the average velocity of the fluid. Thus, the plug zone can span across the channel more quickly resulting in a lower equilibrium height, as seen in figure 2c. In Newtonian fluids, as indicated by previous studies¹⁸, Capillary number (representing the dominance of the viscous forces in contrast to the surface tension forces) has absolutely no effect on the final Jurin height attained; it

just influences the time required for the capillary front to attain that final Jurin height. However In ER fluids, the Capillary number has an influence on the development of the plug zone and thus, on the Jurin height attained. One more important feature of figure 2a is the fact that although for high Capillary numbers, the plug zone spans faster across the channel resulting in a lower Jurin height, it also takes a longer time to evolve as compared to the case of lower Capillary number flow. This result is in accordance with our discussions, since for higher Capillary numbers, the flow is relatively slow and takes longer time to develop. However, owing to the lesser height of the liquid column, the effect of gravity is less pronounced. On the other hand, for lower Capillary numbers, the front attains relatively larger height over shorter time duration (see figure 2c). Therefore, the effect of gravity is more dominant in slowing down the flow, as manifested by a plug zone spanning across the channel. Figure 2(c) clearly depicts that increase in Ca results in lower Jurin height as well as a longer travel time of the meniscus.



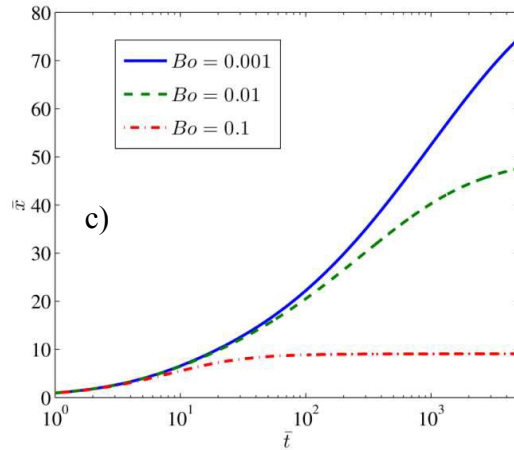
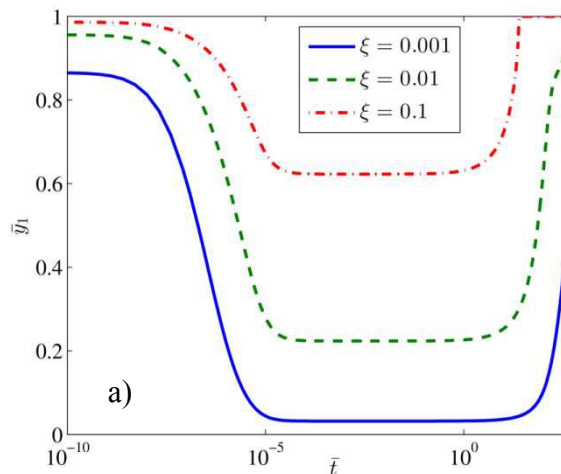


Fig 3. Figure represents the a) development of the dimensionless span of the plug zone \bar{y}_1 measured from the channel centerline; b) variation of dimensionless average velocity of the capillary front \bar{u} ; and c) capillary front advancement \bar{x} as a function of the dimensionless time \bar{t} for different values of Bond number Bo . The other non-dimensional parameters are $Ca=0.1$ $\xi=0.01$.

Figures 3(a) – 3(c) demonstrate the variation of span of the plug zone (fig a), the resulting meniscus velocity (fig b) and the advancement of the capillary front (fig c) with progress of time for different values of Bo , while other relevant parameters have been mentioned in the caption. The trend in the variation of the plug zone span with time is quite similar to figure 2(a). However, with higher Bond number, the span of the plug zone increases faster while the Jurin height attained by the capillary decreases as shown in figures 3a and 3c, respectively. Increase in Bo simply indicates an increase in the gravitational hindrance, which, as expected, results in lower values of Jurin height. The velocity profiles (figure 3b) are also consistent with the flow description wherein the velocity is the lowest for the highest value of Bo .



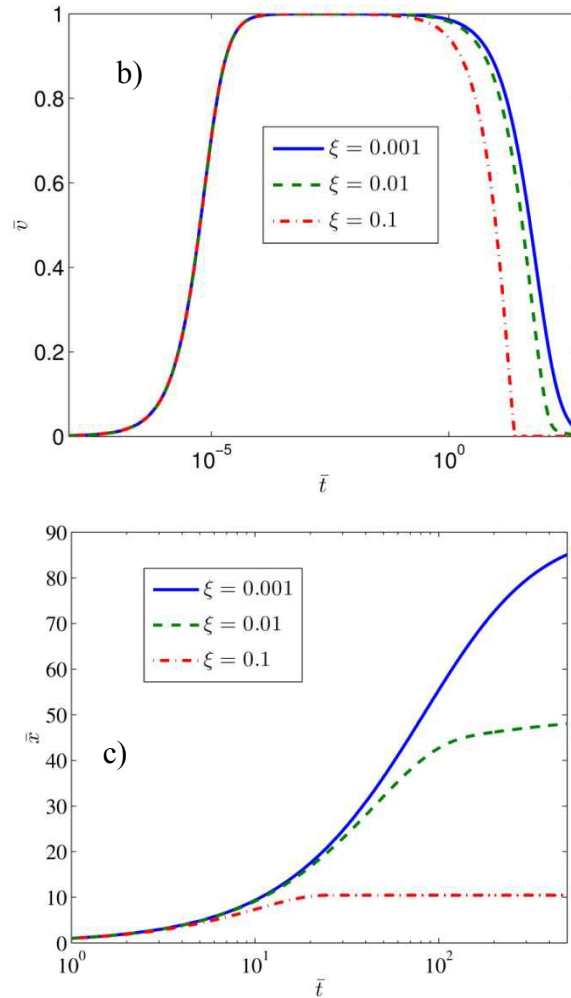


Fig 4. Figure represents the a) development of the dimensionless span of the plug zone \bar{y}_1 measured from the channel centerline; b) variation of dimensionless average velocity of the capillary front \bar{u} ; and c) capillary front advancement \bar{x} as a function of the dimensionless time \bar{t} for different values of the dimensionless number ξ . Other dimensionless parameters are $Bo = 0.01$; $Ca = 0.1$.

Figures 4(a) – 4(c) depict the variation of span of the plug zone (fig a), the meniscus velocity (fig b), and the advancement of the capillary front (fig c) with progress in time for different values of ξ , while the other parameters have been mentioned in the caption. Again we notice here that the trends of the plots are quite similar to figures 2 and 3. It is observed that an increase in ξ increases the yield stress, which results in a higher span of the plug zone across the channel cross-section. As a result of this, the Jurin height also decreases, since the plug zone more effectively spans over the whole cross section. One important point to note from figures 2(a), 3(a) and 4(a) is that during the initial phase of filling, \bar{y}_1 remains strongly dependent on Ca

(fig 2(a)) and ξ (fig 4(a)), whereas its dependence on Bo is very weak, since the curves corresponding to different Bo are nearly overlapped. This can be attributed to the fact that at the initial times of filling, higher Ca signifies a higher viscosity which slows down the flow. A comparatively slower flow means a larger span of the plug zone. Similarly, a higher value of ξ signifies a larger yield stress and a larger span of the plug zone. Thus, variations in Ca and ξ significantly alter the span of the plug zone in the initial times. However, variation of Bo has no effects on the span of the plug zone in the initial times since in this regime, the surface tension and inertial forces are dominant over the gravitational effects.

3.1. Comparison with experiments

We attempt to compare our theoretical results with previously reported experiment on capillary filling of ERFs, performed in ³⁵. The experiments of Korobko *et. al.* ³⁵ were executed with transformer oil as the liquid medium whose density, dielectric constant and surface tension are $\rho_c = 880 \text{ kg/m}^3$, $\varepsilon_c = 2.5$ and $\sigma = 27 \text{ mN/m}$ ³⁵. The conductivity of the continuous phase is found from ⁶¹ in order of 10^{-12} S/m . The density and radius of the suspended particles, as reported in ³⁵, are $\rho_p = 2000 \text{ kg/m}^3$ and $a = 1 \text{ }\mu\text{m}$. The zero-field contact angle estimated from the height data, when no electric field is applied, is $\theta_0 = 76^\circ$. The permittivity of free space is taken as $\varepsilon_0 = 8.85 \times 10^{-12} \text{ F/m}$. The viscosity of transformer oil has the value $\mu_0 = 0.01 \text{ Pa}\cdot\text{s}$ while the viscosity variation with particle concentration is assumed to be of the form $\mu = \mu_0 \left(1 + \frac{5}{2}\phi\right)$ ⁶².

The dielectric constant of SiO_2 particles is generally considered as $\varepsilon_p = 12$ in the low frequency regime (mimicking a DC bias scenario), considering the results reported in ^{63,64} while the DC conductivity is found from ⁶⁵ in order of 10^{-14} S/m . This makes the value of CM factor $\beta \sim 0.5$, estimated based on the conductivity values. We have calculated the yield stress using the equation (1) which comes out in the order of 10 Pa. The contribution factor to the capacitive energy is considered as $w = 9$. The significance of this parameter lies in the fact that in derivation related to electrocapillary effect ^{50,51}, a small dielectric layer is considered near the interface where the electric field is concentrated and therefore the phenomenon of contact angle saturation occurs ⁵⁵. Towards this, we have assumed the correction factor (w) so that the right hand side of equation (8) does not overshoot from unity. It is seen that with this fitting

parameter, the CM, as calculated using the conductivities of the two phase, better predicts the experimental findings as compared to the calculation made by the dielectric constant.

The experiments were conducted by introducing silicon dioxide particles, which alter the surface tension of the fluid medium as well as its density. Therefore, we have assumed the density of the medium to vary in the following way, as a function of particle concentration: $\rho = (1 - \phi)\rho_c + \phi\rho_p$. The variation of the surface tension with particle concentration and particle wetting in presence of an electric field is a complicated study in itself. For the sake of simplicity, we have interpolated the reported values of the surface tension in ³⁵ as a linear function of the particle concentration.

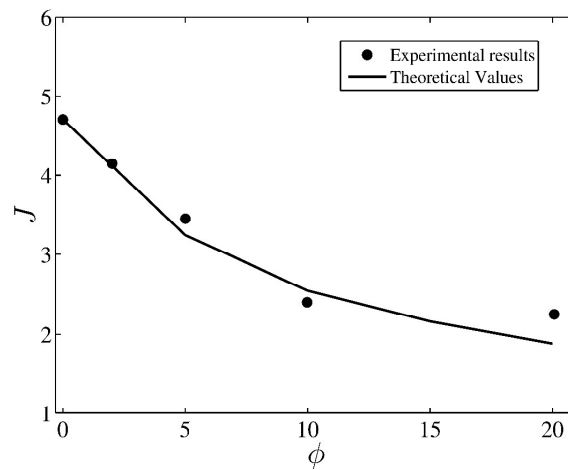


Fig 5. Figure depicts the final Jurin height J (in mm) attained by the capillary front for different particle concentrations ϕ (in % volume fraction of particles) in the suspended medium as obtained from the present theoretical model and a comparison with the experimental results as obtained in ³⁵.

Figure 5 depicts the comparison of the proposed model and experimental findings for the present study. It can be seen that the model predicts the final Jurin height of the ERF capillary rise to a close approximation. For the model, we see that with increase in volume fraction of particles, the effective density of the fluid increases, thereby decreasing the height of the ERF. However, in a counteracting effect, the electric field induced particle wetting increases the effective surface tension, which tends to increase the Jurin height. These two balancing effects determine the equilibrium Jurin height of the ERF within the capillary. It is observed that the influence of particle concentration on the Jurin height is reduced as the volume fraction of the particle in the suspending medium is increased. At higher volume fraction, $\phi > 0.1-0.15$, the

effect of particle-particle interaction is enhanced while the yield stress cannot be accurately predicted resulting in a deviation of our results from the experimental values⁴¹. The prediction of the model can be improved with proper analysis of the particle concentration influence on the surface tension and contact angle while accounting for the variations in density and viscosity induced by the interactions among the particles.

3.2. Scaling Analysis

A: Different Regimes of Capillary Filling

The existence of different regimes due to the effect of the plug zone development over and above the other effects of different forces involved during the capillary front advancement can be qualitatively studied by a thorough scaling analysis of the governing equation. To this end, we note that a sustained capillary filling for a long time would ensure a proper demarcation of the flow regimes attained. For this cause, the effect of gravity is neglected by considering a horizontal channel which ensures a sustained capillary filling for a longer time. The form of the governing equation thus reduces to

$$\underbrace{2H\rho \frac{d}{dt} \left(x \frac{dx}{dt} \right)}_{\Lambda_1} = \underbrace{2\sigma \cos(\theta)}_{\Lambda_2} + \underbrace{\frac{-6\mu H^2}{H^3 - y_1^3} x \frac{dx}{dt}}_{\Lambda_3} + \underbrace{\frac{-3\tau_0 H (H^2 - y_1^2)}{H^3 - y_1^3} x}_{\Lambda_4} \quad (18)$$

The regime at the start of the filling process is a balance between the inertial and surface tension force, i.e. $x \sim t$. This regime has been pointed out in many studies^{17,18,66} and remains valid at early stages of the filling, irrespective of the fluid rheology, as can be seen by balancing the terms Λ_1 and Λ_2 of equation (18). Over this regime, \bar{y}_1 can be scaled using the equation (14). We notice that since $x \sim t$, the velocity scales as unity and thus, from this equation we find that the value of \bar{y}_1 as obtained from $\bar{y}_1^3 - (3 + 6Mn)\bar{y}_1 + 2 \sim 0$, remains almost constant at the initial times which is evident from figure 6.

The next regime is where the surface tension force is balanced by the viscous effects. Here the terms Λ_2 and Λ_3 come into prominence. The effect of the term Λ_4 is not yet felt since the plug zone is confined near the channel centre, which means $\bar{y}_1 \ll O(1)$. Over this regime, it

can be seen that the fluid closely follows the scaling for that of a Newtonian fluid, since the yield stress is less than the shear stress in most of the flow domain. Over this regime, considering

$y_1 \ll H$, $x \sim \sqrt{t}$ from $2\sigma \cos(\theta) \sim \frac{6\mu H^2}{H^3 - y_1^3} \left(\frac{x^2}{t} \right)$ as found by equating term Λ_2 and term Λ_3 .

Thus, the velocity scales as $\sim 1/\sqrt{t}$. Now in this region, equation (14) can be recast by substituting $\bar{y} = 1 - \bar{y}_1$ in

$$3\bar{y}^2 - \bar{y}^3 + \bar{u}6Mn\bar{y} - \bar{u}6Mn = 0 \quad (19)$$

where $\bar{u} \sim \frac{\bar{x}}{\bar{t}} \sim \frac{1}{\sqrt{\bar{t}}}$. We note that, at higher times, $\bar{y}_1 \rightarrow 1$, $\bar{y} \rightarrow 0$. Accordingly, neglecting \bar{y}^3 , the reduced form of equation (19) reads as

$$3\bar{y}^2 + \frac{6Mn}{\sqrt{\bar{t}}}\bar{y} - \frac{6Mn}{\sqrt{\bar{t}}} = 0 \quad (20)$$

The solution of the above equation has the form $\bar{y} = \frac{Mn}{\sqrt{\bar{t}}} \left(\sqrt{1 + \frac{2\sqrt{\bar{t}}}{Mn}} - 1 \right)$. At higher times $\bar{t} \gg 1$

and $Mn \sim O(1)$, we approximate $1 + \frac{2\sqrt{\bar{t}}}{Mn} \approx \frac{2\sqrt{\bar{t}}}{Mn}$ and obtain the final scale of $\bar{y} \sim \sqrt{\frac{2Mn}{\sqrt{\bar{t}}}} - \frac{Mn}{\sqrt{\bar{t}}}$.

Therefore, the dimensionless span of the plug zone scales as $\bar{y}_1 \sim 1 - \sqrt{\frac{2Mn}{\sqrt{\bar{t}}}} + \frac{Mn}{\sqrt{\bar{t}}}$. The scaling

with this equation is plotted in figure 6.

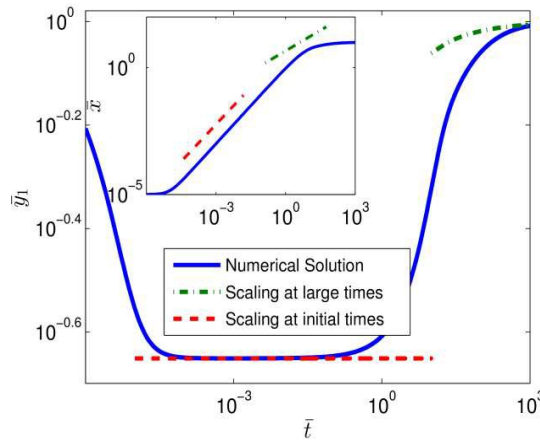


Fig 6. Scaling analysis for the case when $Mn=1$, $Ca=0.1$ and $Bo=0$. The two regimes for the development of the plug zone with progress of time are shown. (Inset) The scaling of the advancement of the capillary front is shown with progress of time for the initial and large time regimes.

Figure 6 depicts the scaling analysis of plug zone span with progress of time. In the inset of figure 6, classical inertial regimes $\bar{x} \sim \bar{t}$ and Washburn regimes $\bar{x} \sim \sqrt{\bar{t}}$ are depicted in comparison to numerical solutions of ER fluids. In the scaling analysis, the effect of inertia on initial time regime shows that the span of the plug zone \bar{y}_1 remains constant as the fluid maintains its maximum velocity for small duration after initial acceleration. Over this regime, the capillary rise \bar{x} scales linearly with \bar{t} , which approximately predicts the capillary height at the initial times, as shown in the figure inset. After the initial transience, the viscous effects come into play and slow down the velocity. The Newtonian part of the flow, where no plug zone has occurred, follows the Washburn regime $\bar{x} \sim \sqrt{\bar{t}}$. However, the average velocity includes the plug zone which does not follow this regime. Thus, at very large times, there is a deviation from the Washburn regime. Nevertheless, the plug zone span, as predicted from the Washburn regime (equation (20)), seems to accurately predict the profile for plug zone development. This is due to the fact that the scaling for Washburn regime holds till the beginning of the plug zone. Thus, exploiting these scaling regimes, one can properly explore how the plug zone develops across the channel height.

B: Capillary entry and Capillary front oscillation

Another important aspect of ER capillary filling would be to predict the conditions under which negligible amount of capillary rise is witnessed by the fluid. In order to estimate such a situation, we have to obtain the yield strength criteria which would obstruct the capillary advancement at very early stages (simulating negligible capillary filling), by balancing the surface tension forces to polarization forces at the capillary entry. It must be appreciated that if the flow has to cease at the entry, the parameter ξ should be the dominating factor, irrespective of the magnitudes of other factors. We assume that an entry length of $\bar{x} = H/10$ can be considered as the scenario where the fluid practically does not enter the capillary (the flow is ceased just at the entrance). For the flow cessation to occur at the entrance, the polarization forces must dominate over the surface tension forces even from the initial stages. Therefore

balancing their contributions we find $\sigma b \leq \tau_0 b \bar{x}$, which reduces to the form $\xi \geq 10$. This can be considered as the criteria for flow cessation.

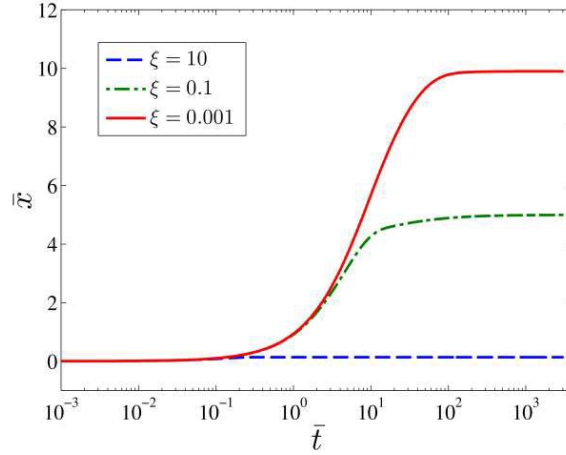


Fig 7. The advancement of the capillary front \bar{x} with dimensionless time for different dimensionless number ξ . The other parameters in this figure are $Bo = 0.1$ and $Ca = 0.1$.

Figure 7 depicts the capillary front dynamics with the passage of time for different values of the dimensionless ξ . ξ signifies the ratio of polarization and surface tension forces. With the above condition we see that for $\theta = 0$ and $Ca = 0.1$, the value of $\xi = 10$ will closely simulate a situation where the filling is completely hindered at the entry of the capillary. As can be seen in the figure, the flow has completely ceased very close to the entry for $\xi = 10$. We have observed that for the same value of ξ and by varying other parameters (Bond and Capillary number), the entry length becomes independent of the other dimensionless numbers at such high magnitudes of ξ ($\xi > 10$).

A vast body of literature^{21,30,31} on capillary filling dynamics discusses the topic of capillary front oscillations about the Jurin height. However, for the case of ER fluids, the capillary front dynamics near the Jurin height has a subtle and distinctive difference in comparison to a classical capillary front dynamics for a Newtonian fluid³¹. For Newtonian fluids, it can be seen that the ratio Ohnesorge number to Bond number in the geometry used in the present study has the form

$$\frac{Oh}{Bo} = \frac{\mu}{\sqrt{\rho\sigma H}} \frac{\sigma}{\rho g H^2}^{31},$$

where, this ratio dictates whether the capillary filling transits to a

viscous (Washburn) regime or oscillatory regime after the initial inertial regime. In the present

context, we see that the ratio of viscous forces to inertial forces scales as $\frac{F_{visc}}{F_{grav}} \sim \frac{3Oh}{Bo} \left(\frac{1}{2Mn} + 1 \right)$.

Thus, we conclude that for the case of capillary filling of ER fluid, the transmission of inertial regime to oscillatory regime or to the Washburn regime is not straightforward and depends on another parameter Mn , known as the Mason number, which signifies the ratio of viscous forces to electrostatic polarization induced forces. For ER fluids, the polarization induced forces are dominant signifying a low Mn ; thus, the fluid is hindered by this additional obstructive effect. This ensures that the dynamical regime of the capillary filling leads directly to the viscous regime from the initial inertial regime due to high viscous forces that are generally associated with ER fluids. In fact an oscillatory regime cannot be observed in capillary filling dynamics of ER fluids. This can be explained based on the simple fact that the particle chains, formed across the capillary gap as soon as the fluid stops completely, would make it impossible for any oscillation to take place (since, for oscillatory mode, the front has to stop and then fall down).

However, with very high Mn , the dominant factor of this regime transition is $\frac{Oh}{Bo}$ as has been

discussed in previous studies³¹. Such a physical paradigm would then lead to a Newtonian like behavior of the front, which can indeed undergo oscillation near the Jurin height. In fact, for short channel length (channel length comparable to Jurin height), the classically observed bulging and oscillation of the fluid near the channel open end for Newtonian rheology, which is

dominated by the parameter We (Weber number $We = \frac{\rho}{8\sigma} x \left(\frac{dx}{dt} \right)^2$)³⁰, is also absent for the case

of ER fluids. In the context of capillary filling of ER fluids, it must be noted that its filling dynamics is generally associated with high contact angle and high viscous effects and, therefore, low filling rates. From the definition of We , we find that the damping in the capillary rise of ER fluids is very high due to viscous effects. In fact, the final height attained will actually be smaller as a result of an additional yield stress associated with such ER flows. The plug zone that will be developed at the channel centerline for the yield stress property of the fluid will not allow the bulging of the fluid in the channel centerline. As a result, a flow with low We signifies that there will not be any vibration in case of short tubes where the capillary front approaches the tube end.

4. Conclusions

In this study, we have investigated the capillary filling dynamics of an Electrorheological Fluid having different concentrations of suspended particles and exposed to different values of the electric field. We have henceforth proposed a theoretical model following reduced order formalism for the capillary front advancement, where the effect of yield stress of the electrorheological fluid and the resulting plug-like zone has been taken into consideration. One critical feature of the theoretical formalism is addressing a non-trivial and complicated interplay between the surface tension and effective viscous forces, both of which depend on the electric field. Another interesting feature of the flow dynamics is the development characteristics of the plug zone and its influence on the final height reached by the capillary front. In this regard, we have demonstrated that the viscosity plays an important role in deciding the final height attained, since a reduction of velocity due to higher viscosity results in augmented development of the plug zone, which in turn, results in a smaller rise of the capillary front. We have also compared our theoretical predictions with previously reported experiments, with reasonable predictive capability. A scaling analysis is also performed for the different regimes of the capillary flow. This analysis reveals that the Washburn regime is shortened due to the yield like action of the fluid. This action may eventually arrest any motion when the whole fluid domain has a shear rate that is less as compared to the yield stress of the fluid for the corresponding electric field. A similar dynamical phenomenon may occur in another class of smart fluids known as magnetorheological fluids. The fluid mainly constitutes of magnetic particles that orient themselves and chain along the magnetic field direction^{67,68}. Magnetorheological fluids can also exhibit capillary filling and the trends can be quite similar to the dynamics of ER fluids. Nevertheless, the mechanism behind its rheological variation is different and holds a merit for an independent investigation. We believe that our results may be of importance towards designing smart capillary filling systems in which electric field and flow rheology may simultaneously act as modulating parameters.

References

- 1 M. Parthasarathy and D. Klingenberg, *Mater. Sci. Eng. R Reports*, 1996, **17**, 57–103.
- 2 C. F. Zukoski, *Annu. Rev. Mater. Sci.*, 1993, **23**, 45–78.

- 3 W. Wen, X. Huang, S. Yang, K. Lu and P. Sheng, *Nat. Mater.*, 2003, **2**, 727–30.
- 4 P. Sheng and W. Wen, *Annu. Rev. Fluid Mech.*, 2012, **44**, 143–174.
- 5 Y. D. Liu and H. J. Choi, *Soft Matter*, 2012, **8**, 11961–11978.
- 6 W. M. Winslow, *J. Appl. Phys.*, 1949, **20**, 1137–1140.
- 7 V. I. Kordonsky, *J. Rheol. (N. Y. N. Y.)*, 1991, **35**, 1427–1439.
- 8 J. Trlica, O. Quadrat, V. Bradna, P. Pavlínek and P. Sába, *J. Rheol. (N. Y. N. Y.)*, 1996, **40**, 943–946.
- 9 C. R. Daubert, J. F. Steffe and A. K. Srivastava, *J. Food Process Eng.*, 1998, **21**, 249–261.
- 10 L. Bitman, Y.-T. Choi and N. M. Wereley, *J. Intell. Mater. Syst. Struct.*, 2002, **13**, 633–639.
- 11 J. A. Marins, B. G. Soares, A. A. Silva, M. G. Hurtado and S. Livi, *J. Colloid Interface Sci.*, 2013, **405**, 64–70.
- 12 C. Li, J. Huang, Q. Tang, J. Huang, J. Zhang and L. Zhou, *Soft Matter*, 2012, **8**, 5250–5255.
- 13 M. S. Cho, H. J. Choi and M. S. Jhon, *Polymer (Guildf.)*, 2005, **46**, 11484–11488.
- 14 T. Hao, *Adv. Colloid Interface Sci.*, 2002, **97**, 1–35.
- 15 R. Lucas, *Kolloid-Zeitschrift*, 1918, **23**, 15–22.
- 16 E. W. Washburn, *Phys. Rev.*, 1921, **17**, 273–283.
- 17 D. Quéré, *Europhys. Lett.*, 1997, **39**, 533–538.
- 18 A. Hamraoui and T. Nylander, *J. Colloid Interface Sci.*, 2002, **250**, 415–21.
- 19 S. Chakraborty, *Anal. Chim. Acta*, 2007, **605**, 175–84.
- 20 N. Desai, U. Ghosh and S. Chakraborty, *Phys. Rev. E*, 2014, **89**, 063017-1 - 063017-13.
- 21 A. Bandopadhyay, U. Ghosh and S. Chakraborty, *Phys. Rev. E*, 2014, **89**, 053024-1 - 053024-10.
- 22 P. Goswami and S. Chakraborty, *Int. J. Micro-Nano Scale Transp.*, 2014, **5**, 23–38.

- 23 T. Andruk, D. Monaenkova, B. Rubin, W.-K. Lee and K. G. Kornev, *Soft Matter*, 2014, **10**, 609–15.
- 24 F. Chauvet, S. Geoffroy, A. Hamoumi, M. Prat and P. Joseph, *Soft Matter*, 2012, **8**, 10738–10749.
- 25 G. Martic, F. Gentner, D. Seveno, D. Coulon, J. De Coninck and T. D. Blake, *Langmuir*, 2002, **18**, 7971–7976.
- 26 N. Fries and M. Dreyer, *J. Colloid Interface Sci.*, 2008, **320**, 259–63.
- 27 S. Chakraborty, *Lab Chip*, 2005, **5**, 421–30.
- 28 B. M. Mognetti and J. M. Yeomans, 2010, **6**, 2400–2402.
- 29 S. Das, P. R. Waghmare and S. K. Mitra, *Phys. Rev. E*, 2012, **86**, 067301-1 - 067301-5.
- 30 O. Shardt, P. R. Waghmare, J. J. Derksen and S. K. Mitra, *RSC Adv.*, 2014, **4**, 14781–14785.
- 31 S. Das and S. K. Mitra, *Phys. Rev. E*, 2013, **87**, 063005-1 - 063005-7.
- 32 P. R. Waghmare and S. K. Mitra, *Microfluid. Nanofluidics*, 2012, **12**, 53–63.
- 33 P. Joos, P. Van Remoortere and M. Bracke, *J. Colloid Interface Sci.*, 1990, **136**, 189–197.
- 34 R. M. Digilov, *Langmuir*, 2008, **24**, 13663–7.
- 35 E. V. Korobko, R. G. Gorodkin, M. I. Mardosevich, E. I. Mardosevich and A. O. Korobko, *Int. J. Mod. Phys. B*, 2005, **19**, 1388–1394.
- 36 K. G. Kornev and A. V Neimark, *J. Colloid Interface Sci.*, 2003, **262**, 253–62.
- 37 K. R. Rajagopal and A. S. Wineman, *Acta Mech.*, 1992, **91**, 57–75.
- 38 R. J Hunter, *Zeta potential in colloid science: principles and applications*, London ; New York : Academic Press, 1981., 1981.
- 39 R. F. Probstein, *Physicochemical Hydrodynamics*, John Wiley & Sons, Inc., Hoboken, NJ, USA, 1994.
- 40 S. Das, S. Chanda, J. C. T. Eijkel, N. R. Tas, S. Chakraborty and S. K. Mitra, *Phys. Rev. E*, 2014, **90**, 043011-1 - 043011-11.
- 41 D. J. Klingenberg and C. F. Zukoski, *Langmuir*, 1990, **6**, 15–24.

- 42 P. Atten, C. Boissy, J.-N. Foulc and K. Q. Zhu, *J. Intell. Mater. Syst. Struct.*, 1996, **7**, 573–578.
- 43 H. J. H. Clercx and G. Bossis, *J. Chem. Phys.*, 1995, **103**, 9426–9437.
- 44 K. Zhang, Y. D. Liu, M. S. Jhon and H. J. Choi, *J. Colloid Interface Sci.*, 2013, **409**, 259–63.
- 45 T. B. Jones, *Electromechanics of Particles*, Cambridge University Press, Cambridge, 1995.
- 46 W. Wen, X. Huang and P. Sheng, *Soft Matter*, 2008, **4**, 200–210.
- 47 L. C. Davis, *J. Appl. Phys.*, 1992, **72**, 1334–1340.
- 48 W. Eckart, *Contin. Mech. Thermodyn.*, 2000, **12**, 341–362.
- 49 A. Ursescu, Technische Universität Darmstadt, Germany, 2005.
- 50 T. B. Jones, *Langmuir*, 2002, **18**, 4437–4443.
- 51 J. H. Chen and W. H. Hsieh, *J. Colloid Interface Sci.*, 2006, **296**, 276–83.
- 52 L. L. Schramm and L. G. Hepler, *Can. J. Chem.*, 1994, **72**, 1915–1920.
- 53 B. P. Binks and S. O. Lumsdon, *Langmuir*, 2000, **16**, 8622–8631.
- 54 D. Bonn, J. Eggers, J. Indekeu, J. Meunier and E. Rolley, *Rev. Mod. Phys.*, 2009, **81**, 739–805.
- 55 A. Quinn, R. Sedev and J. Ralston, *J. Phys. Chem. B*, 2005, **109**, 6268–75.
- 56 R. Shamaï, D. Andelman, B. Berge and R. Hayes, *Soft Matter*, 2008, **4**, 38–45.
- 57 Y. Wang and Y.-P. Zhao, *Soft Matter*, 2012, **8**, 2599–2606.
- 58 L. Y. Yeo and H.-C. Chang, *Mod. Phys. Lett. B*, 2005, **19**, 549–569.
- 59 J. R. Dormand and P. J. Prince, *J. Comput. Appl. Math.*, 1980, **6**, 19–26.
- 60 P. Bogacki and L. F. Shampine, *Appl. Math. Lett.*, 1989, **2**, 321–325.
- 61 A. Ciuriuc, P. V. Notingher, M. Jovalekic and S. Tenbohlen, in *2014 International Conference on Optimization of Electrical and Electronic Equipment (OPTIM)*, 2014, pp. 169–174.

- 62 L. G. Leal, *Advanced Transport Phenomena*, Cambridge University Press, Cambridge, 2007.
- 63 T. Tepper and S. Berger, *Nanostructured Mater.*, 1999, **11**, 1081–1089.
- 64 K. Dutta and S. K. De, *J. Nanoparticle Res.*, 2006, **9**, 631–638.
- 65 J. K. Srivastava, M. Prasad and J. B. Wagner, Jr., *J. Electrochem. Soc.*, 1985, 132, 955.
- 66 A. A. Duarte, *Am. J. Phys.*, 1996, **64**, 413–418.
- 67 E. M. Furst and A. P. Gast, *Phys. Rev. E - Stat. Physics, Plasmas, Fluids, Relat. Interdiscip. Top.*, 2000, **61**, 6732–6739.
- 68 T. Butz and O. von Stryk, *ZAMM*, 2002, **82**, 3–20.